



# CHORUS

This is the accepted manuscript made available via CHORUS. The article has been published as:

## Tunable Nonreciprocal Quantum Transport through a Dissipative Aharonov-Bohm Ring in Ultracold Atoms

Wei Gou, Tao Chen, Dizhou Xie, Teng Xiao, Tian-Shu Deng, Bryce Gadway, Wei Yi, and Bo Yan

Phys. Rev. Lett. **124**, 070402 — Published 20 February 2020

DOI: [10.1103/PhysRevLett.124.070402](https://doi.org/10.1103/PhysRevLett.124.070402)

# Tunable non-reciprocal quantum transport through a dissipative Aharonov-Bohm ring in ultracold atoms

Wei Gou,<sup>1,\*</sup> Tao Chen,<sup>1,\*</sup> Dizhou Xie,<sup>1</sup> Teng Xiao,<sup>1</sup> Tian-Shu Deng,<sup>2</sup> Bryce Gadway,<sup>3</sup> Wei Yi,<sup>4,5,†</sup> and Bo Yan<sup>1,6,7,‡</sup>

<sup>1</sup>*Interdisciplinary Center of Quantum Information,  
State Key Laboratory of Modern Optical Instrumentation,  
and Zhejiang Province Key Laboratory of Quantum Technology and Device  
of Physics Department, Zhejiang University, Hangzhou 310027, China*

<sup>2</sup>*Institute for Advanced Study, Tsinghua University, Beijing, 100084, China*

<sup>3</sup>*Department of Physics, University of Illinois at Urbana-Champaign, Urbana, IL 61801-3080, USA*

<sup>4</sup>*CAS Key Laboratory of Quantum Information, University of Science and Technology of China, Hefei 230026, China*

<sup>5</sup>*CAS Center For Excellence in Quantum Information and Quantum Physics, Hefei 230026, China*

<sup>6</sup>*Collaborative Innovation Centre of Advanced Microstructures, Nanjing University, Nanjing, 210093, China*

<sup>7</sup>*Key Laboratory of Quantum Optics, Chinese Academy of Sciences, Shanghai, 200800, China*

(Dated: January 21, 2020)

We report the experimental observation of tunable, non-reciprocal quantum transport of a Bose-Einstein condensate in a momentum lattice. By implementing a dissipative Aharonov-Bohm (AB) ring in momentum space and sending atoms through it, we demonstrate a directional atom flow by measuring the momentum distribution of the condensate at different times. While the dissipative AB ring is characterized by the synthetic magnetic flux through the ring and the laser-induced loss on it, both the propagation direction and transport rate of the atom flow sensitively depend on these highly tunable parameters. We demonstrate that the non-reciprocity originates from the interplay of the synthetic magnetic flux and the laser-induced loss, which simultaneously breaks the inversion and the time-reversal symmetries. Our results open up the avenue for investigating non-reciprocal dynamics in cold atoms, and highlight the dissipative AB ring as a flexible building element for applications in quantum simulation and quantum information.

Quantum transport, a fundamental property and a key probe of quantum many-body systems, lies at the core of seminal discoveries in condensed-matter physics such as superconductivity [1] and topological materials [2, 3]. Besides reciprocal transport, where the transfer function of energy or particle between two points in space is symmetric in the direction of flow, non-reciprocal transport also exists in various physical contexts, and finds applications in electric diodes, non-reciprocal optical, optomechanical device [4–15], and non-linear metamaterials [16, 17]. Understanding and controlling non-reciprocal quantum transport is of fundamental importance for the study of many-body dynamics [18, 19], the quantum simulation of exotic models [20, 21], and the design of useful quantum device for quantum information [22–26].

With flexible controls and versatile detection schemes, quantum gases have proved to be an important physical platform for the study of quantum transport [27–33]. For example, superfluidity in multiple-connected geometries has been investigated using a Bose-Einstein condensate (BEC) in ring traps [34, 35], and quantized conductance has been reported for the transport of cold atoms through a point contact [36, 37]. However, non-reciprocal quantum transport has yet to be implemented with cold atoms, where the interplay of non-reciprocity and the highly tunable parameters of the many-body system *per se* holds fascinating potentials for both quantum simulation and quantum information [38, 39].

In this work, we report the experimental observation of non-reciprocal quantum transport of a BEC through a

dissipative Aharonov-Bohm (AB) ring. Coupling discrete momentum states using multi-frequency Bragg lasers, we implement a dissipative AB ring on a momentum lattice, where both the synthetic magnetic flux through the ring and the laser-induced loss on the ring are easily tunable. By measuring the atomic momentum distribution at different times, we experimentally probe the transport of atoms through the AB ring, and observe a parameter-dependent, directional atom flow, which originates from the interplay of the synthetic magnetic flux and the laser-induced loss.

*Implementing dissipative AB ring:*— As illustrated in Fig. 1(a), the key element for non-reciprocal transport, the dissipative AB ring, consists of a closed triangle with three lattice sites. The synthetic magnetic flux is generated by the phases of the hopping terms along the triangle. The on-site loss with a rate  $\gamma$  on the vertex of the triangle makes the AB ring dissipative. To demonstrate the non-reciprocal transport, we perform numerical simulations on the time evolution of a single-particle initialized to the left or right of the ring on the lattice [40]. As shown in Fig. 1(b), atom transport can be made unidirectional under the parameters  $\gamma/t = 1$  and  $\phi = 3\pi/2$ , i.e., they are only allowed to propagate through the ring when injected from the left. Note that directional transport from the right to the left is also possible by choosing different parameters  $\gamma$  and  $\phi$ .

Our experimental configuration is schematically illustrated in Fig. 1(c). Starting with a BEC of  $6 \times 10^4$  <sup>87</sup>Rb atoms in a weak crossed-dipole trap with trapping

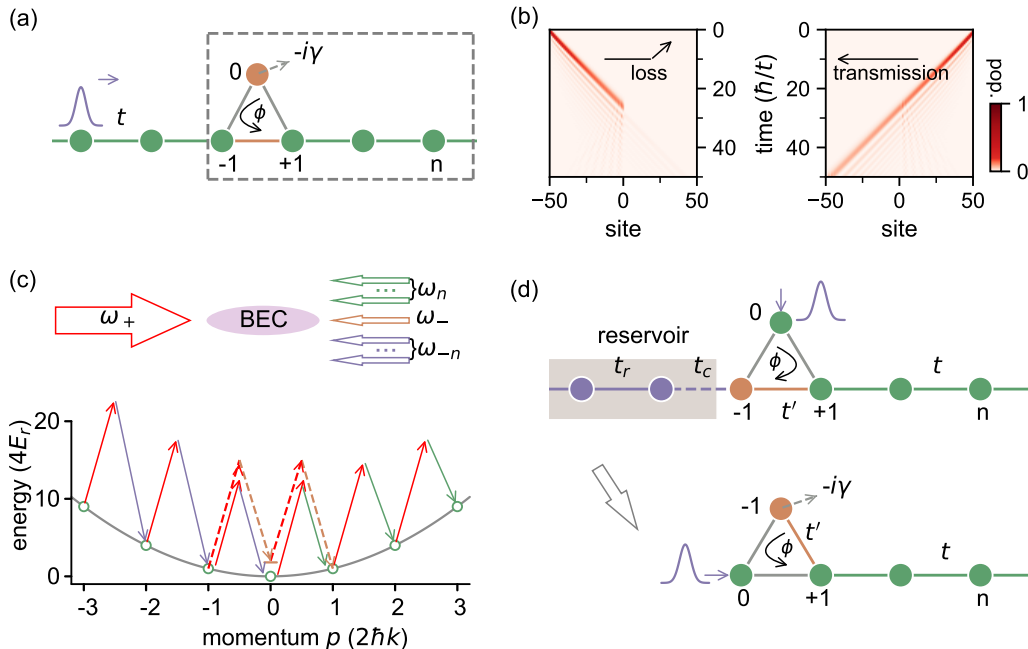


FIG. 1. (a) Schematic illustration of a dissipative AB ring (the 3-site triangle within the dashed box) along a lattice. The green, grey, and orange bonds correspond to hopping rates  $t$ ,  $t e^{-i\phi/2}$ , and  $t'$ , respectively, between adjacent sites. The vertex of the ring (site 0 in orange) features an on-site loss with rate  $\gamma$ . (b) Numerical simulation of non-reciprocal atom transport through the AB ring in (a), where we initialize atoms on the lattice sites  $\pm 50$  to the left or right of the ring, and plot the time-dependent population distribution [40]. We fix  $\gamma/t = 1$  and  $\phi = 3\pi/2$  for the calculation, in which case atoms incoming from the left are lost to the reservoir through site 0, whereas atoms incoming from the right can transport through. (c) Illustration of the experimental implementation of the momentum lattice and the AB ring. The momentum lattice is formed with multiple pairs of two-photon Bragg transitions (solid arrows), while momentum states  $|n = 1\rangle$  is coupled to  $|n = -1\rangle$  with a four-photon second-order Bragg process (dashed arrows). Here the frequency components  $\omega_n$  of the left-going Bragg laser satisfies  $\omega_n = \omega_+ - 4(2n + 1)E_r/\hbar$ , while  $\omega_- = \omega_+$ . (d) Implementation of on-site loss and the mapping of the system to (a). The left side of the lattice with  $n < -1$  is mapped to a reservoir, with hopping rate  $t_r$  within the reservoir and  $t_c$  between the system and the reservoir. The laser-induced hopping rate between momentum states  $| - 1\rangle$  and  $| 1\rangle$  is  $t'$ , which allows us to map  $| - 1\rangle$  to lattice site 0 in (a) with an effective loss rate  $\gamma \approx t_c^2/t_r$ .

frequencies  $2\pi \times (115, 40, 100)\text{Hz}$  [41], we create a one-dimensional momentum lattice along the  $y$ -direction, using a series of two-photon Bragg transitions to couple discrete momentum states  $|n\rangle$  ( $n \in \mathbb{Z}$ ) [33, 42, 43]. The Bragg transitions are driven by counter-propagating, far-detuned laser pairs with the wavelength  $\lambda = 1064$  nm, whose multi-frequency components (with frequencies  $\omega_n$ ) are generated by acoustic optical modulators (AOMs). The resulting discrete momentum state  $|n\rangle$  along the lattice has the momentum  $p = 2n\hbar k$  ( $k = 2\pi/\lambda$ ), and the single-photon recoil energy  $E_r = (\hbar k)^2/2m = h \times 2.03\text{kHz}$ , with  $m$  the atomic mass. As the nearest-neighbour sites are coupled by resonant Bragg transitions, we fix the effective Rabi frequency such that  $t = h \times 1.25(2)\text{kHz}$  throughout our experiment. Under these conditions, the interaction effects on the dynamics is negligible [40].

To close the ring, we couple the momentum states  $|n = -1\rangle$  and  $|n = 1\rangle$  using a four-photon process with the effective coupling rate  $t' = h \times 1.26(4)\text{kHz}$ . The four-

photon process is induced by a pair of lasers with frequencies  $\omega_{\pm}$  ( $\omega_+ = \omega_-$ ), as shown in Fig. 1(c) [44, 45]. Denoting the relative phases of the frequency components  $\{\omega_-, \omega_{0,-1}\}$ , with respect to  $\omega_+$ , as  $\{\phi_-, \phi_{0,-1}\}$ , we implement the synthetic magnetic flux  $\phi$  by setting  $\phi_- = 0$  and  $\phi_0 = \phi_{-1} = -\phi/2$ . We also introduce detunings for different frequency components, to compensate for the site-dependent Stark shifts induced by off-resonant Bragg transitions [40].

To implement the on-site loss, we use the left side of the lattice ( $n < -1$ ) as a reservoir. As shown in Fig. 1(d), the laser-induced hopping rate is  $t_r = t$  within the reservoir, whereas the hopping rate between sites  $| - 1\rangle$  and  $| - 2\rangle$  is  $t_c$ . The loss mechanism is best understood in the extreme limit of  $t_c \ll t_r$ , where it takes a long time for a coherent population exchange between the system ( $n \geq -1$ ) and the reservoir ( $n < -1$ ). Any population of the reservoir is therefore considered as loss during this period. It follows from the second-order perturbation that the effective on-site loss rate for  $| - 1\rangle$  at short times is  $\gamma \approx t_c^2/t_r$  [46].

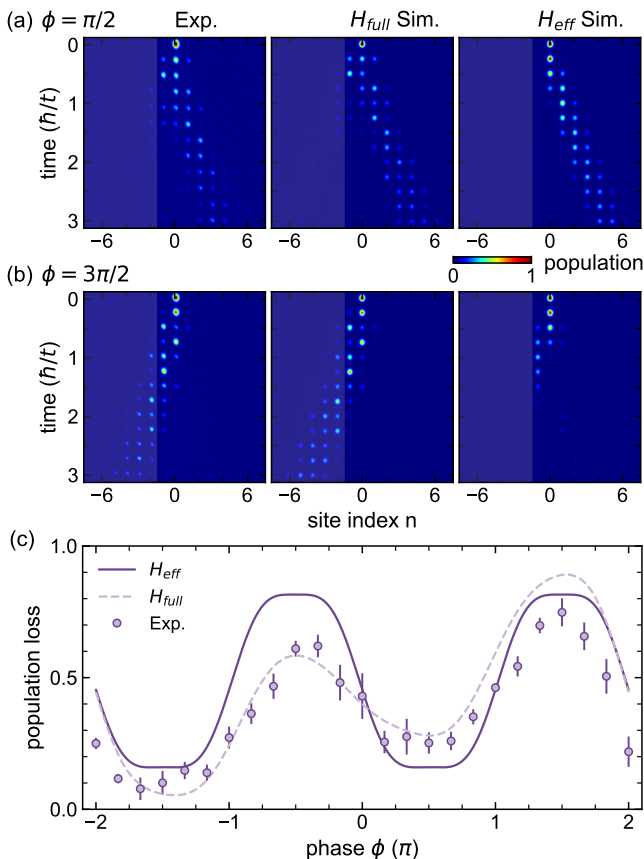


FIG. 2. (a)(b) Phase-dependent transport for (a)  $\phi = \pi/2$ , and (b)  $\phi = 3\pi/2$ . From left to right, the panels are experimental data, numerical simulation using the full Hamiltonian, and simulation using the effective Hamiltonian [40]. The masked regions correspond to the reservoir. (c) The population loss  $\mathcal{P}_\ell$  as a function of  $\phi$ , after an evolution time of  $3\hbar/t$ . Experimental data are shown as purple dots with error bars. The dashed line is from the numerical simulation with the full Hamiltonian, and the solid line is the prediction from the effective Hamiltonian (1). For all cases, we fix the effective loss rate  $\gamma/t = 1$ , and initialize the BEC on site  $|0\rangle$ .

While  $\gamma$  would deviate from  $t_c^2/t_r$  beyond the regime  $t_c \ll t_r, t$ , as we show later, the effective Hamiltonian derived therein provides a qualitatively correct picture for our experimental observations. Finally, in the experiment, all the parameters  $t, t', t_c$  and  $t_r$  can be independently tuned by adjusting the laser intensities for the corresponding frequency component [40].

With these, the effective Hamiltonian of the dissipative AB ring is written as

$$H_{\text{eff}} = -i\gamma c_{-1}^\dagger c_{-1} + \left[ \sum_{n \geq 1} t c_n^\dagger c_{n+1} + t e^{-i\frac{\phi}{2}} c_{-1}^\dagger c_0 + t e^{-i\frac{\phi}{2}} c_0^\dagger c_1 + t' c_1^\dagger c_{-1} + \text{H.c.} \right], \quad (1)$$

where  $c_n$  ( $c_n^\dagger$ ) is the annihilation (creation) operator on site  $n$  of the momentum lattice. Here we neglect the

higher-order, off-resonant couplings, which are included in a time-dependent full Hamiltonian. The Stark shifts of these off-resonant couplings, however, are compensated by shifting the frequencies, as we discuss earlier [40].

*Tunable non-reciprocal transport:*— We first investigate the special case with an effective loss rate  $\gamma = t$  for a 15-site chain, with the BEC naturally initialized on the momentum-lattice site  $|0\rangle$ . We show the measured momentum-space density distribution at different evolution times in Figs. 2(a) ( $\phi = \pi/2$ ) and 2(b) ( $\phi = 3\pi/2$ ), where the reservoir region is masked. The experimental data fit qualitatively well with numerical simulations, and the dynamics on the momentum lattice is quite different for different values of  $\phi$ . When  $\phi = \pi/2$ , transmission dominates: BEC atoms pass through the dissipative AB ring to populate lattice sites with  $n > 1$  [Fig. 2(a)]. In contrast, when  $\phi = 3\pi/2$ , loss dominates: BEC atoms are blocked by the ring, leaving lattice sites with  $n > 1$  mostly unpopulated. Our observation is therefore consistent with the directional transport illustrated in Fig. 1(b).

Next, we characterize transport properties of the ring by tuning the flux parameter  $\phi$ . To quantitatively analyze the phase-dependent transport, we introduce the population loss  $\mathcal{P}_\ell$ , defined as the total population in the reservoir

$$\mathcal{P}_\ell = \sum_{n < -1} \rho_n, \quad (2)$$

where  $\rho_n$  is the population of the momentum state  $|n\rangle$ . Intuitively,  $\mathcal{P}_\ell$  measures the atom population lost to the reservoir: transmission (loss) dominates when  $\mathcal{P}_\ell$  is small (large). For our experiment, we measure  $\mathcal{P}_\ell$  after an evolution time  $\tau = 3\hbar/t$  ( $\sim 384 \mu\text{s}$ ) for different values of the flux parameter  $\phi$ . As shown in Fig. 2(c),  $\mathcal{P}_\ell$  oscillates with varying  $\phi$ , reflecting a sensitive dependence of the transport behavior on the flux. Specifically, the measured  $\mathcal{P}_\ell$  suggests a transmission-dominant behavior at  $\phi = \pi/2$ , and a loss-dominant behavior at  $\phi = 3\pi/2$ . Our experimental observation clearly demonstrates that the transport through the dissipative AB ring is non-reciprocal. This is because atoms passing through the AB ring to the right with the flux parameter  $\phi$  and atoms passing to the left with  $2\pi - \phi$  are reverse processes, as their corresponding terms in Hamiltonian (1) are Hermitian conjugate to each other up to a gauge transformation. Such a non-reciprocity originates from the interplay of the synthetic flux and the on-site loss, which simultaneously break inversion and time-reversal symmetries.

As shown in Fig. 2, our measurements agree qualitatively well with numerical simulations under the effective Hamiltonian (solid line) and the full Hamiltonian (dashed line), with the data typically in better agreement with the full-Hamiltonian simulation, due to the inclusion of higher-order, off-resonance processes. However, an exception can be observed near  $\phi = 3\pi/2$ , where

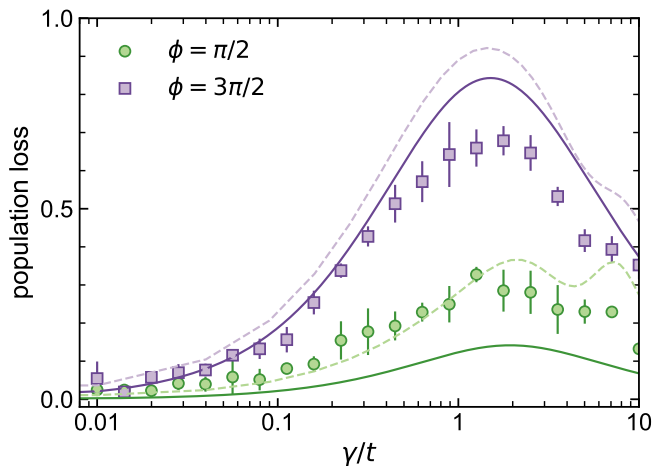


FIG. 3. Dependence of the population loss  $\mathcal{P}_\ell$  on the effective loss rate  $\gamma$ . Two data sets are shown, with the synthetic magnetic flux  $\phi = \pi/2$  (green circles) and  $3\pi/2$  (purple squares), respectively. We also show results from numerical simulations using the effective (solid lines) and the full Hamiltonians (dashed lines). For all cases, the evolution time is taken to be  $\tau = 3\hbar/t$ .

considerable deviation occurs between our measurements and the full-Hamiltonian simulation. Such a deviation is attributed to the experimental imperfections at large population loss which tend to underestimate the atom loss [40]. We note that the difference in  $\mathcal{P}_\ell$  at  $\phi = 0, \pm 2\pi$  under the full-Hamiltonian simulation originates from higher-order, off-resonant couplings.

*Impact of the on-site loss:*— We now explore the dependence of the atom transport on the on-site loss rate  $\gamma$ . With a fixed hopping rates  $t_r = t$  and by tuning  $t_c$  from  $0.01t$  to  $4t$ , we are able to change  $\gamma/t$  by 3 orders of magnitude. Figure 3 shows two sets of experimental measurements with  $\phi = \pi/2$  and  $\phi = 3\pi/2$ , respectively. For both measurements,  $\mathcal{P}_\ell$  peaks at an intermediate  $\gamma/t \sim 1$ , where it is most sensitive to the flux parameter  $\phi$ , as discussed above. Again, the deviation of the experimental data from the full-Hamiltonian simulation near  $\gamma/t = 1$  for  $\phi = 3\pi/2$  is due to experimental imperfection at large population loss [40]. Further, our experimental data fit quantitatively better with numerical simulations for  $\gamma/t < 0.1$ , which is easier to understand, since the expression  $\gamma \approx t_c^2/t_r$  is no longer a good approximation for large  $\gamma/t$ .

Physically, the loss dependence of the transport can be understood as follows. In the weak-coupling regime with  $t_c \rightarrow 0$ , site  $|-1\rangle$  is effectively disconnected from the reservoir; whereas in the strong coupling regime, quantum Zeno effect suppresses the population loss [47]. Thus, the non-reciprocal transport can only occur when  $\gamma$  is neither too small nor too large. Our experiments reveals that the interplay of the synthetic magnetic flux and the on-site loss gives rise to the non-reciprocal trans-

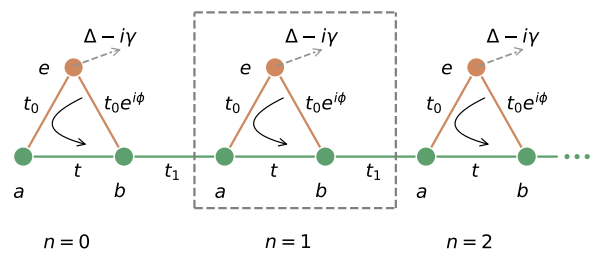


FIG. 4. Schematic illustration of a lattice with coupled dissipative AB rings.

port of the dissipative AB ring.

*Discussions and outlook:*— The dissipative AB rings demonstrated here can find useful applications in quantum simulation and quantum information. As a concrete example and outlook, we now discuss in more detail the possibility of simulating highly non-trivial non-Hermitian topological models using dissipative AB rings.

We consider a series of coupled dissipative AB rings, with hopping rates  $t_0$ ,  $t$  and  $t_1$  as indicated in Fig. 4. Besides the on-site loss with rate  $\gamma$ , the vertices of the rings also feature an energy offset  $\Delta$ . The alternating hopping rates  $t$  and  $t_1$  along the lattice divide the system into unit cells (labeled by  $m$ ) consisting of sublattice sites (labeled by  $a$  and  $b$ ). Such a model, as we argue below, is analogous to the non-Hermitian SSH model studied in Ref. [48]. An outstanding feature of such a non-Hermitian model is the presence of non-Hermitian skin effects, where all eigenstates of the system under the open-boundary condition become localized at boundaries. The skin effects also give rise to the breakdown of the conventional bulk-boundary correspondence, a fundamentally important phenomenon unique to non-Hermitian topological systems which has stimulated intense theoretical and experimental studies [48–54]. Key to the non-Hermitian SSH model is the non-reciprocal hopping between two sublattice sites within a unit cell, which, in our case, is guaranteed by the non-reciprocal transport of the dissipative AB ring. A qualitative understanding of the proposed setup can be obtained in the weak-coupling limit ( $t_0 \ll \Delta, \gamma, t$ ), where the effective Hamiltonian reads (setting  $\phi = \pi/2$ ) [40]

$$H_{\text{skin}} = \sum_m [\tilde{\Delta}(c_{m,a}^\dagger c_{m,a} + c_{m,b}^\dagger c_{m,b}) + (t + \tilde{\gamma})c_{m,a}^\dagger c_{m,b} + (t - \tilde{\gamma})c_{m,b}^\dagger c_{m,a} + t_1(c_{m+1,a}^\dagger c_{m,b} + \text{H.c.})]. \quad (3)$$

Here  $c_{m,a(b)}$  ( $c_{m,a(b)}^\dagger$ ) is the annihilation (creation) operator for the  $a(b)$  sublattice in the  $m$ th unit cell, the complex Stark shift  $\tilde{\Delta}$  and the complex differential hopping rate  $\tilde{\gamma}$  are functions of  $t_0$ ,  $\Delta$  and  $\gamma$  [40]. Equation (3) is similar to the non-Hermitian SSH model in Ref. [48], only with additional complex energy-shift terms on the sublattice sites and a complex  $\tilde{\gamma}$ . We have numerically

checked that, under the open-boundary condition, the model in Fig. 4 features non-Hermitian skin effects and the breakdown of conventional bulk-boundary correspondence, even for parameters beyond the weak-coupling regime [40]. Building upon the experimental scheme reported here, the configuration in Fig. 4 can be readily implemented in cold atoms using a two-component BEC, with one component prepared in the momentum lattice, and the other subject to laser-induced loss [55]. The intra- and inter-species hoppings can be induced by Bragg lasers or by microwave fields.

*Conclusion:*— With highly tunable, non-reciprocal transport properties, dissipative AB rings are useful building blocks for applications in quantum simulation and quantum information. Our experiment not only lays the groundwork for investigating non-reciprocal many-body dynamics in cold atoms, but also prepares for the simulation of intriguing non-Hermitian physics or the design of useful quantum device in the quantum many-body setting of cold atoms.

*Acknowledgement:*— We thank Professor Youquan Li and Lihua Lv for helpful discussions. We acknowledge support from the National Key R&D Program of China under Grant Nos. 2018YFA0307200, 2016YFA0301700 and 2017YFA0304100. National Natural Science Foundation of China under Grant Nos. 91636104, 11974331 and 91736209. Natural Science Foundation of Zhejiang province under Grant No. LZ18A040001, and the Fundamental Research Funds for the Central Universities. B.G. acknowledges support from the National Science Foundation under Grant No. 1707731.

---

\* These authors contributed equally to this work

† [wyz@ustc.edu.cn](mailto:wyz@ustc.edu.cn)

‡ [yanbohang@zju.edu.cn](mailto:yanbohang@zju.edu.cn)

- [1] B. T. Matthias, T. H. Geballe, and V. B. Compton, *Rev. Mod. Phys.* **35**, 1 (1963).
- [2] M. Z. Hasan and C. L. Kane, *Rev. Mod. Phys.* **82**, 3045 (2010).
- [3] X. L. Qi and S. C. Zhang, *Rev. Mod. Phys.* **83**, 1057 (2011).
- [4] D. L. Sounas and A. Alù, *Nat. Photon.* **11**, 774 (2017).
- [5] Y. Shoji and T. Mizumoto, *Sci. Technol. Adv. Mater.* **15**, 014602 (2014).
- [6] A. Metelmann and A. A. Clerk, *Phys. Rev. X* **5**, 021025 (2015).
- [7] P. Lodahl, S. Mahmoodian, S. Stobbe, A. Rauschenbeutel, P. Schneeweiss, J. Volz, H. Pichler, and P. Zoller, *Nature* **541**, 473 (2017).
- [8] H. Li, Y. Y. Huang, X. Z. Zhang, and L. Tian, *Opt. Express* **25**, 18907 (2017).
- [9] D. Malz, L. D. Tóth, N. R. Bernier, A. K. Feofanov, T. J. Kippenberg, and A. Nunnenkamp, *Phys. Rev. Lett.* **120**, 023601 (2018).
- [10] Z. Shen, Y.-L. Zhang, Y. Chen, F.-W. Sun, X. B. Zou, G.-C. Guo, C.-L. Zou, and C.-H. Dong, *Nat. Commun.* **9**, 1797 (2018).
- [11] B. Lei, J. Hu, P. Jiang, D. H. Kim, G. F. Dionne, L. C. Kimerling, and C. A. Ross, *Nat. Photon.* **5**, 758 (2011).
- [12] D.-W. Wang, H.-T. Zhou, M.-J. Guo, J.-X. Zhang, J. Evers, and S.-Y. Zhu, *Phys. Rev. Lett.* **110** (2013).
- [13] C. Javaherian and J. Twamley, *Opt. Exp.* **25**, 025970 (2017).
- [14] S. Longhi, *Opt. Lett.* **40**, 1278 (2015).
- [15] L. Jin and Z. Song, *Phys. Rev. Lett.* **121**, 073901 (2018).
- [16] C. Coulais, D. Sounas, and A. Alù, *Nature* **542**, 461 (2017).
- [17] L. Feng, Y.-L. Xu, W. S. Fegadolli, M.-H. Lu, J. E. B. Oliveira, V. R. Almeida, Y.-F. Chen, and A. Scherer, *Nat. Mater.* **12**, 108 (2013).
- [18] L. Duca, T. Li, M. Reitter, I. Bloch, M. Schleier-Smith, and U. Schneider, *Science* **347**, 288 (2015).
- [19] A. Seif, W. DeGottardi, K. Esfarjani, and M. Hafezi, *Nat. Commun.* **9**, 1207 (2018).
- [20] T. Ozawa, H. M. Price, A. Amo, N. Goldman, M. Hafezi, L. Lu, M. C. Rechtsman, D. Schuster, J. Simon, O. Zeitlinger, and I. Carusotto, *Rev. Mod. Phys.* **91**, 015006 (2019).
- [21] E. Mascarenhas, F. Damanet, S. Flannigan, L. Tagliacozzo, A. J. Daley, J. Gould, and I. de Vega, *Phys. Rev. B* **99**, 245134 (2019).
- [22] K. Stannigel, P. Komar, S. J. M. Habraken, S. D. Bennett, M. D. Lukin, P. Zoller, and P. Rabl, *Phys. Rev. Lett.* **109**, 013603 (2012).
- [23] J. Kim, M. C. Kuzyk, K. Han, H. Wang, and G. Bahl, *Nat. Phys.* **11**, 275 (2015).
- [24] D. L. Hurst, D. M. Price, C. Bentham, M. N. Makhonin, B. Royall, E. Clarke, P. Kok, L. R. Wilson, M. S. Skolnick, and A. M. Fox, *Nano Lett.* **18**, 5475 (2018).
- [25] S. Barzanjeh, M. Aquilina, and A. Xuereb, *Phys. Rev. Lett.* **120**, 060601 (2018).
- [26] H. Li, T. Kottos, and B. Shapiro, *Phys. Rev. Applied* **9**, 044031 (2018).
- [27] J. Billy, V. Josse, Z. Zuo, A. Bernard, B. Hambrecht, P. Lugan, D. Clement, L. Sanchez-Palencia, P. Bouyer, and A. Aspect, *Nature* **453**, 891 (2008).
- [28] S. S. Kondov, W. R. McGehee, J. J. Zirbel, and B. DeMarco, *Science* **334**, 66 (2011).
- [29] M. Schreiber, S. S. Hodgman, P. Bordia, H. P. Lueschen, M. H. Fischer, R. Vosk, E. Altman, U. Schneider, and I. Bloch, *Science* **349**, 842 (2015).
- [30] L. W. Clark, A. Gaj, L. Feng, and C. Chin, *Nature* **551**, 356 (2017).
- [31] T. Haug, H. Heimonen, R. Dumke, L.-C. Kwek, and L. Amico, *Phys. Rev. A* **100**, 041601 (2019).
- [32] L. Feng, J. Hu, L. W. Clark, and C. Chin, *Science* **363**, 521 (2019).
- [33] E. J. Meier, F. A. An, and B. Gadway, *Phys. Rev. A* **93**, 051602 (2016).
- [34] S. Eckel, J. G. Lee, F. Jendrzejewski, N. Murray, C. W. Clark, C. J. Lobb, W. D. Phillips, M. Edwards, and G. K. Campbell, *Nature* **506**, 200 (2014).
- [35] S. Eckel, F. Jendrzejewski, A. Kumar, C. J. Lobb, and G. K. Campbell, *Phys. Rev. X* **4**, 031052 (2014).
- [36] C. C. Chien, S. Peotta, and M. Di Ventra, *Nat. Phys.* **11**, 998 (2015).
- [37] S. Häusler, S. Nakajima, M. Lebrat, D. Husmann, S. Krinner, T. Esslinger, and J.-P. Brantut, *Phys. Rev. Lett.* **119**, 030403 (2017).
- [38] F. Damanet, E. Mascarenhas, D. Pekker, and A. J. Da-

- ley, *Phys. Rev. Lett.* **123**, 180402 (2019).
- [39] H. Xu, L. Jiang, A. A. Clerk, and J. G. E. Harris, *Nature* **568**, 65 (2019).
- [40] See Supplementary Materials for details..
- [41] D. Xie, D. Wang, W. Gou, W. Bu, and B. Yan, *J. Opt. Soc. Am. B* **35**, 500 (2018).
- [42] F. A. An, E. J. Meier, and B. Gadway, *Sci. Adv.* **3**, e1602685 (2017).
- [43] D. Xie, W. Gou, T. Xiao, B. Gadway, and B. Yan, *npj Quantum Information* **5**, 1 (2019).
- [44] E. Giese, A. Roura, G. Tackmann, E. M. Rasel, and W. P. Schleich, *Phys. Rev. A* **88**, 053608 (2013).
- [45] F. A. An, E. J. Meier, J. Ang'ong'a, and B. Gadway, *Phys. Rev. Lett.* **120**, 040407 (2018).
- [46] S. Lapp, J. Ang'ong'a, F. A. An, and B. Gadway, *New J. Phys.* **21**, 045006 (2019).
- [47] W. M. Itano, D. J. Heinzen, J. J. Bollinger, and D. J. Wineland, *Phys. Rev. A* **41**, 2295 (1990).
- [48] S. Yao and Z. Wang, *Phys. Rev. Lett.* **121**, 086803 (2018).
- [49] T. E. Lee, *Phys. Rev. Lett.* **16**, 133903 (2016).
- [50] F. K. Kunst, E. Edvardsson, J. C. Budich, and E. J. Bergholtz, *Phys. Rev. Lett.* **121**, 026808 (2018).
- [51] C. H. Lee and R. Thomale, *Phys. Rev. B* **99**, 201103(R) (2019).
- [52] L. Xiao, T.-S. Deng, K. Wang, G. Zhu, Z. Wang, W. Yi, and P. Xue, arXiv:1907.12566 (2019).
- [53] T. Helbig, T. Hofmann, S. Imhof, M. Abdelghany, Klessling, T., L. W. Molenkamp, L. C. H., A. Szameit, M. Greiter, and R. Thomale, arXiv:1907.11562 (2019).
- [54] A. Ghatak, M. Brandenbourger, J. van Wezel, and C. Coulais, arXiv:1907.11619 (2019).
- [55] J. Li, A. K. Harter, J. Liu, L. de Melo, Y. N. Joglekar, and L. Luo, *Nat. Commun.* **10**, 855 (2019).